

Electronic and Geometric Structure of the Cluster Compound $\text{Au}_{55}[\text{P}(\text{C}_6\text{H}_5)_3]_{12}\text{Cl}_6$. A Computational Study

Alexander Genest, Sven Krüger, and Notker Rösch

Technische Universität München, Department Chemie and Catalysis Research Center, 85747 Garching, Germany

Reprint requests to Prof. N. Rösch. E-Mail: roesch@mytum.de

Z. Naturforsch. **2009**, *64b*, 1246–1258; received September 13, 2009

Dedicated to Professor Hubert Schmidbaur on the occasion of his 75th birthday

Relativistic density functional calculations have been carried out on the model cluster $\text{Au}_{55}(\text{PH}_3)_{12}\text{Cl}_6$ assuming a cuboctahedral or an icosahedral Au_{55} metal core to model the experimentally suggested cluster compound assigned as $\text{Au}_{55}[\text{P}(\text{C}_6\text{H}_5)_3]_{12}\text{Cl}_6$. Besides the overall shape of the metal core, the study focused on the unresolved issue at which sites the chlorine ligands are attached. The calculations reproduce characteristic interatomic distances within ~ 2 pm, with the exception of the Au–Cl bonds. Chlorine ligands were calculated to prefer higher coordinated sites whereas the previously postulated on-top coordination at the center of the Au (100) facets of a cuboctahedron was found to be unstable. In fact, the present model results suggest an ensemble of several higher coordinated sites. The often assumed cuboctahedral shape of the metal cluster core was determined to be slightly less stable than an approximately icosahedral shape. The calculations allow a rationalization of the difficulties faced in experiments that attempted to discriminate cluster isomers.

Key words: DFT Calculations, Au_{55} , Cluster Compound, Metal Ligand Interaction

Introduction

Small metal particles are important as building blocks of nanostructured materials [1–4]. Metal clusters often are stabilized by a protective shell of ligands because bare metal species agglomerate easily or incorporate impurities [2,3]. Despite being decorated by ligands, these clusters still may be viewed as models for catalytically active small metal particles [3]. For instance, gold cluster catalysts with particle diameters from 1.4 nm, *i. e.* with 55 and more gold atoms, have recently been reported as very active in the transfer of oxygen [5–8]. Ligands affect the preferred nuclearity and therefore are often introduced during the synthesis of metal particles to control the nucleation process [1–3]. A notable example is the cluster compound assigned as $\text{Au}_{55}[\text{P}(\text{C}_6\text{H}_5)_3]_{12}\text{Cl}_6$ to which this study is devoted [9]. In fact, it was proposed [9,10] that clusters of a specific nuclearity are generated when one reduces $(\text{C}_6\text{H}_5)_3\text{PAuCl}$ with B_2H_6 in benzene at 50 °C. Stable monodisperse cluster systems of this size are quite rare [1,2], yet very interesting for building up nanostructured systems with precise size-dependent properties.

Originally, a cuboctahedral structure was postulated for $\text{Au}_{55}[\text{P}(\text{C}_6\text{H}_5)_3]_{12}\text{Cl}_6$ [9]. As a cuboctahedron features 12 corners and 6 facets, it is suggestive to assign the phosphine ligands to corner sites and the chlorine ligands to locations at the centers of the (100) facets [9]. The Au_{55} cluster compound did not yield crystals suitable for X-ray crystallographic studies [10], but extended X-ray fine structure spectroscopy (EXAFS) furnished Au–Au nearest-neighbor distances of 275–280 pm [11–13]. The result Au–Au = (278.5 ± 0.3) pm with the smallest error range [13] agrees very well with the average nearest-neighbor distance, 279 pm, calculated with the local density approximation (LDA) for a bare cuboctahedral cluster Au_{55} [14]; the corresponding value for bare Au_{55} with icosahedral symmetry constraints was 281 pm [14]. These values are noticeably shorter than the experimental nearest-neighbor distance of bulk gold, 288 pm [15] in line with the well known scaling of interatomic distances of metal clusters [14]. A study using another method based on Density Functional Theory (DFT), employing a plane-wave approach in combination with the gradient-corrected exchange-correlation functional PW91, de-

terminated an average Au–Au distance of 288 pm for cuboctahedral Au₅₅ and 290 pm for the corresponding bare icosahedral species [16].

The Au–Au coordination numbers from different EXAFS studies scatter notably (7.8 [12], 7.6 [11], 6.5 [13]) with uncertainties ranging from 0.4 to 1. An ideal cuboctahedron of 55 atoms exhibits an average coordination number of 7.85; for an icosahedron of the same nuclearity, the average value is slightly larger, 8.51 [14]. Note that one EXAFS investigation was able to resolve more than a single shell of Au–Au distances [11]. For the second shell at 393 pm, the coordination number was determined to 5.0 ± 8 ; for the third shell at 488 pm the coordination number was 0.60 ± 0.5 .

Early on, results of mass spectroscopy on the Au₅₅[P(C₆H₅)₃]₁₂Cl₆ sample were alternatively interpreted as comprising Au₆₇ moieties with a structure where six icosahedral Au₁₃ moieties are interconnected by 11 vertices [17, 18]. An ideal icosahedral cluster features intershell Au–Au bonds that are 5% shorter than its *intrashell* bonds, at variance with an ideal octahedral cluster where tangential and radial bonds are equally long. EXAFS was able to resolve these two different bond lengths for the icosahedral cluster Au₁₁L₇I₃, but not for Au₅₅[P(C₆H₅)₃]₁₂Cl₆ [11]. Therefore, an icosahedral shape of the Au₅₅ moiety was ruled out [11]. Further studies on the nuclearity of the metal core of Au₅₅[P(C₆H₅)₃]₁₂Cl₆ claimed that either such cluster samples contained a size distribution or prevailing experimental conditions destroyed the mononuclearity [19–22]. In particular, X-ray exposure in spectroscopic experiments was shown to decompose the ligand shell [23, 24]. As a result, the structure of this particular cluster compound and the dispersion of the size of the metal core, even the existence of a definite compound as such, remained controversial till today [11, 13, 17–22, 24–27].

From the decomposition enthalpy, 1590 kJ mol^{-1} , of Au₅₅[P(C₆H₅)₃]₁₂Cl₆, measured at 156 °C, a binding energy of 76 kJ mol^{-1} per Au–Au bond was estimated [28]. This calorimetric measurement involves a destructive reaction, which can be triggered thermally and happens as a “strong sharp exothermic decomposition” [28]. This finding was taken as additional signature of a well-defined compound [28]. From IR spectroscopy the frequency of the Au–Cl stretching vibration of Au₅₅[P(C₆H₅)₃]₁₂Cl₆ was determined at 280 cm^{-1} while the reactant of the synthe-

sis, (C₆H₅)₃PAuCl, exhibits this mode at 330 cm^{-1} [9]. Also electronic properties of the cluster compound Au₅₅[P(C₆H₅)₃]₁₂Cl₆ were intensely studied, *e. g.*, at the energy range close to the Fermi level with UV/Vis spectroscopy [23] and by X-ray photoemission spectroscopy on selected Au 4*f* core levels [23, 29–38]. The claimed removal of the chlorine ligands increases the intensity of photoelectron spectra in the vicinity of the Fermi level by a factor of 6 (from close to zero), rendering it similar to the intensity measured for a gold film [23]; this change in the electronic structure was interpreted as an insulator-to-metal transition [23].

In summary, despite extensive experimental effort, the structure of the metal moiety of Au₅₅[P(C₆H₅)₃]₁₂Cl₆ as well as crucial aspects of metal-metal and metal-ligand bonding remained open. In the following we report quantum chemical calculations on this cluster compound that were carried out to assist the interpretation of experimental findings.

Computational Method and Models

We carried out all-electron calculations with the linear combination of Gaussian-type orbitals fitting-functions density-functional (LCGTO-FF-DF) method [39] as implemented in the program PARAGAUSS [40, 41]. Scalar relativistic effects were taken into account self-consistently with the Douglas-Kroll-Hess (DKH) approach to the Dirac-Kohn-Sham problem [42–44]. All calculations were performed in spin-unrestricted fashion. Structures were optimized at the LDA level [45]. Subsequently, at these LDA equilibrium geometries, binding energies were calculated self-consistently with the gradient-corrected exchange-correlation functional proposed by Becke and Perdew (BP; generalized gradient approximation, GGA) [46, 47]. This “single-point” strategy provides sufficiently accurate binding energies in a very efficient manner [48]. Often, especially for systems with many heavy-element atoms, LDA yields more accurate results for bond lengths, whereas GGA functionals in general provide more reliable energetic parameters [49–51]. Vertical ionization potentials (IPs) and electron affinities (EAs) as well as other features of the electronic structure were determined at the GGA level. For the numerical integration of the exchange-correlation contributions, we used a superposition of atom-centered spherical grids [52] that in the angular coordinates are accurate up to angular momentum $L = 19$ [53]. These grids comprised about 16000 points for

an Au center, 12000 for Cl and P centers, and 7000 for H centers.

The Kohn-Sham orbitals were represented by flexible Gaussian-type basis sets [54], contracted in a generalized fashion. For Au, a (19s, 15p, 10d, 6f) basis set was contracted to [9s, 8p, 5d, 2f]. For P and Cl, (12s, 9p, 1d) basis sets were contracted to [6s, 5p, 1d]. For H, the contraction (6s, 1p) → [4s, 1p] was chosen. In the LCGTO-FF-DF method, the Hartree contribution to the electron-electron interaction is evaluated by representing the electronic charge density with an auxiliary Gaussian-type basis set [39]. The functions of s- and r²-type of this auxiliary set were constructed in a standard fashion by scaling the exponents of the orbital basis sets [39]. In addition, five p- and five d-type “polarization” exponents (except for H) were added on each atom, chosen as geometric series with factors of 2.5, starting at 0.1 and 0.2 au, respectively. Thus, the auxiliary basis set was of the size (19s, 7r², 5p, 5d) for Au, (12s, 9r², 5p, 5d) for P and Cl, and (6s, 1r², 5p) for H.

In the SCF calculations, the elements of the density matrix were converged to at least 10⁻⁸ au. Geometries were considered to be converged when the maximum component of the energy gradient and the optimization step had dropped below 10⁻⁵ au.

The average binding energy BE(*X*) of a ligand *X* at the cluster Au₅₅ was determined as

$$\text{BE}(X) = E_{\text{tot}}[X] + \{E_{\text{tot}}[\text{Au}_{55}] - E_{\text{tot}}[\text{Au}_{55}X_n]\}/n$$

where E_{tot} is the total energy of a system. In the compound Au₅₅X_{*n*}Y_{*m*} with two sets of ligands *X* and *Y*, we estimated the binding energy BE(*X*) accordingly, *i. e.*, by formally substituting Au₅₅Y_{*m*} for Au₅₅ in the equation above. We estimated the basis set superposition error of Au–Cl bonds by comparison with ClAuPH₃ where the counterpoise method [55] yielded a value below 2 kJ mol⁻¹.

To render accurate electronic structure calculations feasible for such large systems we modeled the cluster compound Au₅₅[P(C₆H₅)₃]₁₂Cl₆ as Au₅₅(PH₃)₁₂Cl₆, invoking simplified phosphine ligands and certain symmetry constraints (see below). We refer to the various coordination modes of chlorine as μ_1 for terminal, μ_2 for bridge, and μ_3 for hollow coordination. As a second label of a structure, we use the symmetry constraints imposed on the calculation. Isomers of the same type of chlorine coordination are discriminated by labels α and β . For example, Au₅₅(PH₃)₁₂(μ_3 -Cl)₆S₆ α denotes one of the isomers calculated

Table 1. Properties of Au₅₅ clusters in O_h, S₆, and I_h symmetry.

Symmetry	O _h	I _h	S ₆
$\langle \text{Au-Au} \rangle^a$, pm	277.4	280.0	280.3
M ^b	2	4	2
$\Delta\epsilon^c$, eV	0.22	0.90	0.14
IP ^d , eV	6.31	6.13	6.18
EA ^e , eV	4.09	3.88	3.93
E_{rel}^f , kJ mol ⁻¹	6.6	20.8	0.0
E_{bond}^g , kJ mol ⁻¹	64	59	59
n^h	216	234	234

^a Average Au–Au bond length; ^b ground state spin multiplicity; ^c HOMO-LUMO gap; ^d ionization potential; ^e electron affinity; ^f energy difference to the most stable structure S₆; ^g binding energies per Au–Au bond; ^h number of Au–Au bonds.

with S₆ symmetry where chlorine ligands are coordinated at hollow sites.

Results and Discussion

As reference, we will first discuss results for the bare model cluster Au₅₅ when different symmetry constraints are imposed. Then we discuss the effect of using model phosphine ligands PH₃ instead of triphenylphosphine P(C₆H₅)₃. Next, we address chlorine coordination at various sites of an Au₅₅ cluster. Finally, we present the results for the fully ligated cluster model Au₅₅(PH₃)₁₂Cl₆.

Model cluster Au₅₅

We first optimized the structure of Au₅₅ as a cuboctahedron using O_h symmetry constraints (Table 1). A calculation using the subgroup D_{2d} of O_h, not shown in Table 1, gave essentially identical results. Starting the geometry optimization with a cuboctahedral cluster, but imposing the reduced symmetry S₆, resulted in a distorted icosahedral structure where each original (100) facet is broken along a diagonal into two triangular facets, yielding 20 triangular faces in total (Fig. 1). Recall that the group S₆ is a subgroup of the icosahedral group I_h [56]. Finally, we also determined the structure of Au₅₅ as an icosahedron using I_h symmetry constraints (Table 1).

The average nearest-neighbor distance of the Au₅₅ cuboctahedron (O_h) was calculated at 277.4 pm, while the icosahedral model yielded 280.0 pm. The distorted icosahedral structure with S₆ symmetry exhibits a slightly longer average Au–Au distance, 280.3 pm (Table 1). The O_h and S₆ structures feature a doublet ground state while the ideal icosahedral model has a quartet electronic state with a singly occupied degenerate HOMO, 66 g¹, that is expected to undergo a Jahn-

Table 2. Structural characteristics of ClAuPR_3 from X-ray diffraction crystal structures, EXAFS experiments, and calculations. Also shown are measured and calculated frequencies of the Au–Cl mode.

R	C_6H_5 EXAFS ^a	C_6H_5 XRD ^b	CH_3 XRD ^c	CH_3 calcd. ^d	H calcd. ^d
Au–P, pm	221.4	223.5	223.3	222.3	221.2
Au–Cl, pm	227.7	227.9	231.0	224.5	223.1
Au–C, pm	3.7	3.4	–	3.406	–
$\nu(\text{Au–Cl})^e$, cm^{-1}	330 ^f	–	312 ^g	350	386

^a Ref. [62]; ^b ref. [63]; ^c ref. [64]; ^d present work; ^e vibrational frequencies of Au–Cl modes; ^f ref. [9]; ^g ref. [65].

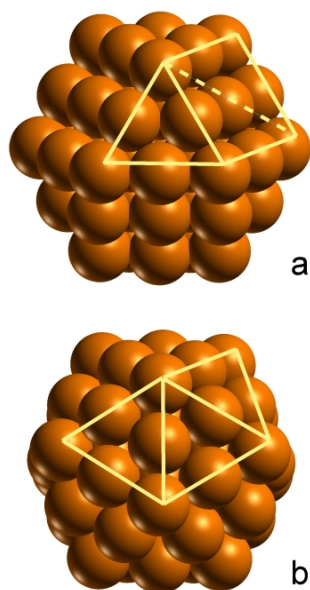


Fig. 1. Au_{55} cluster of cuboctahedral and quasi-icosahedral shape. a) Au_{55} in O_h symmetry, oriented in the same way as species with constraints according to S_6 symmetry; b) Au_{55} in S_6 symmetry adopting a quasi-icosahedral shape; note the distortion of the (100) facet at the top right of this structure.

Teller distortion. The I_h structure has also the largest HOMO-LUMO gap, 0.9 eV, while the cuboctahedron exhibits a gap of 0.22 eV and the distorted icosahedral S_6 species a gap of 0.14 eV. The ionization potential and the electron affinity vary only slightly with the structure, 6.2 ± 0.1 eV and 4.0 ± 0.1 eV, respectively (Table 1).

The quasi-icosahedral S_6 structure yields the lowest total energy; the O_h structure lies 6.6 kJ mol^{-1} , the ideal I_h structure 20.8 kJ mol^{-1} higher in energy. Therefore, the three structures are expected to transform easily into each other under the influence of a ligand environment. The binding energy per Au atom is 251 kJ mol^{-1} for each of the three shapes whereas the binding energy E_{bond} per Au–Au bond varies by $\sim 10\%$ among the different structures, from 64 to 59 kJ mol^{-1} (Table 1). However, this variation is sim-

ply a consequence of the fact that the number of bonds varies with the shape.

In a previous study [14] relying on GGA geometries optimized with a more flexible basis set, the icosahedral structure was calculated 265 kJ mol^{-1} more stable than the cuboctahedral shape, which translates into a difference of $\sim 5 \text{ kJ mol}^{-1}$ in the binding energies per atom. As the present study aims at larger systems and systems of low symmetry, we chose a less flexible basis set. A recent DFT study [16], using the PW91 exchange-correlation functional with a plane-wave approach, determined the icosahedral shape 106 kJ mol^{-1} more stable than the octahedral one. A tight binding approach [57] predicted this energy preference of the icosahedral structure at 26 kJ mol^{-1} . While studying symmetric model systems one should keep in mind that there is also computational evidence for amorphous structures of Au_{55} clusters [58–60].

Phosphine ligands on Au_{55}

The effect of replacing the triphenylphosphine groups $\text{P}(\text{C}_6\text{H}_5)_3$ of $\text{Au}_{55}[\text{P}(\text{C}_6\text{H}_5)_3]_{12}\text{Cl}_6$ by simple phosphines PH_3 was checked on the molecule $[\text{P}(\text{C}_6\text{H}_5)_3]\text{AuCl}$. An earlier study had quantified the effect of such a simplification for the molecule $(\text{CH}_3)\text{AuPR}_3$, $R = \text{H}, \text{CH}_3$, and C_6H_5 [61]. There the model with the simple phosphine was found to reproduce the Au–CH₃ bond length of 202 pm within 3 pm, and the corresponding ligand binding energy, 436 kJ mol^{-1} , within 1%.

Table 2 shows that bond lengths of $[\text{P}(\text{C}_6\text{H}_5)_3]\text{AuCl}$ from X-ray diffraction and EXAFS data agree within 1% [62]. When PH_3 is used as model ligand, the Au–P distance of $[\text{P}(\text{C}_6\text{H}_5)_3]\text{AuCl}$, calculated at 221.2 pm, is reproduced with a 1% deviation whereas the Au–Cl bond is calculated 2% too short compared to experiment. The stretching frequency $\nu(\text{Au–Cl})$, 386 cm^{-1} , derived from a full normal mode analysis, overestimates the experimental result, 330 cm^{-1} [9]. Thus, for this bond the electron do-

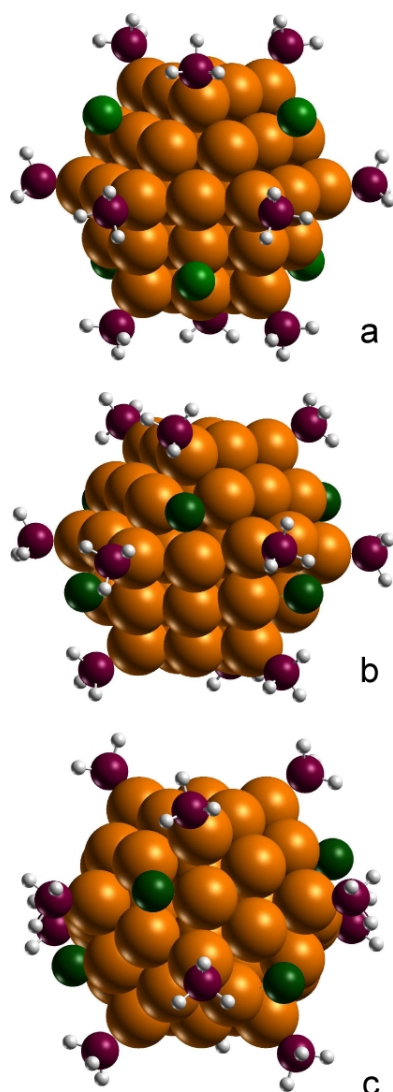


Fig. 2. Optimized cluster models: a) $\text{Au}_{55}(\text{PH}_3)_{12}(\mu_1\text{-Cl})_6$ D_{2d} ; b) $\text{Au}_{55}(\text{PH}_3)_{12}(\mu_3\text{-Cl})_6$ $S_6\alpha$; c) $\text{Au}_{55}(\text{PH}_3)_{12}(\mu_3\text{-Cl})_6$ $S_6\beta$.

nating effect of the $\text{P}(\text{C}_6\text{H}_5)_3$ ligand may play a notable role. To check this, we also studied trimethylphosphine $\text{P}(\text{CH}_3)_3$ as ligand where methyl groups act as stronger electron donating substituents than hydrogen in PH_3 . Indeed, the Au–P bond of $[\text{P}(\text{CH}_3)_3]\text{AuCl}$ matches the value of the crystal structure of $[\text{P}(\text{C}_6\text{H}_5)_3]\text{AuCl}$, with a deviation of only 1.2 pm [63], whereas the Au–Cl bond is calculated only slightly longer, by 1.4 pm, than with the simple phosphine, matching the experimental value within 1.5 % (Table 2). Also the calculated Au–Cl vibrational frequency, 350 cm^{-1} , is notably re-

duced, deviating 20 cm^{-1} from the experimental value for $[\text{P}(\text{C}_6\text{H}_5)_3]\text{AuCl}$.

The Au–Cl bond of $[\text{P}(\text{CH}_3)_3]\text{AuCl}$ is calculated 6.5 pm shorter than in the corresponding crystal structure (Table 2) [64]. This deviation may be a packing effect of the crystal structure, where the molecules are oriented to form trimer chains with Au–Au distances of at least 355 pm. In addition to the elongated Au–Cl distances, this feature of the crystal structure may also rationalize the low vibrational Au–Cl frequency of 312 cm^{-1} [64,65]. In view of this argument, one may wonder about the close reproduction of the Au–P distance; note, however, that the Au–P bond length hardly changes with the substituents R of PR_3 , R = phenyl, methyl, H (Table 2).

Overall, we consider PH_3 as adequate model for studying the effects of phosphine ligation on Au_{55} , but the length of Au–Cl bonds may be slightly underestimated. Following the early structure model for $\text{Au}_{55}[\text{P}(\text{C}_6\text{H}_5)_3]_{12}\text{Cl}_6$ [9], we calculated cuboctahedral Au_{55} with 12 model ligands PH_3 coordinated at the corner atoms, as assumed in the experiment [9], imposing symmetry according to the subgroup D_{2d} of O_h (see above). Although 10 pm longer than the Au–P bond of $\text{ClAu}(\text{PH}_3)$ (Table 2), the resulting Au–P distance, 231 pm, of $\text{Au}_{55}(\text{PH}_3)_{12}$ fits very well the corresponding EXAFS result, $230 \pm 2\text{ pm}$ [11, 13], for $\text{Au}_{55}[\text{P}(\text{C}_6\text{H}_5)_3]_{12}\text{Cl}_6$. The increased Au–P distance is in line with the higher Au coordination of the ligation site in $\text{Au}_{55}(\text{PH}_3)_{12}$ (Fig. 2). Bond competition with the PH_3 ligands also increases the Au–Au distances of these site atoms, by 3 pm to 275 pm. The average Au–Au bond length of $\text{Au}_{55}(\text{PH}_3)_{12}$, 278 pm, is 1 pm larger than in Au_{55} .

The 12 PH_3 ligands strongly affect the IP and EA values of the system, which are reduced by 1.7 and 1.5 eV, respectively, compared to bare Au_{55} . A Mulliken analysis indicates a small total transfer, $\sim 0.3\text{ e}$, of electron density from the ligand shell to the Au_{55} core. The binding energy per PH_3 ligand on Au_{55} , 71 kJ mol^{-1} , is rather small compared to the atomization energy per Au atom, 251 kJ mol^{-1} , of the bare cluster, but slightly stronger than its average Au–Au bond, $\sim 64\text{ kJ mol}^{-1}$. In view of previous results [61], one would expect that $\text{P}(\text{C}_6\text{H}_5)_3$ binds stronger to Au_{55} than PH_3 . However, steric effects in $\text{Au}_{55}[\text{P}(\text{C}_6\text{H}_5)_3]_{12}\text{Cl}_6$ may destabilize the binding of the latter ligand. In summary, one can expect PH_3 to yield adequate estimates of the phosphine binding in $\text{Au}_{55}[\text{P}(\text{C}_6\text{H}_5)_3]_{12}\text{Cl}_6$.

Table 3. Calculated properties of $\text{Au}_{55}\text{Cl}_6$ complexes where the chlorine ligands move along a path that preserves D_{3d} symmetry^a.

φ^b , deg	54.5	60	66	68.7	90.1	111.4
Coordination ^c	top on center			bridge	top on edge	hollow
Facet	100	100	100	100	100, 111	111
$\text{Au}^1\text{-Cl}^d$, pm	234.3	234.7	239.4	245.6	230.7	255.5
$\text{Au}^2\text{-Cl}^e$, pm	376.3	316.1	257.5	245.9	451.7	256.6
$\langle\text{Au-Au}\rangle^f$, pm	278.3	278.6	279.2	279.5	278.3	281.1
BE^g , kJ mol^{-1}	204	213	241	246	210	234
ν^h , cm^{-1}	285, 32i, 60i			244, 163, 42	308, 54, 148i	218, 123, 105
$q(\text{Cl}_6)^i$, e	-1.6	-1.4	-1.0	-0.9	-1.5	-0.5

^a See Fig. 3a,b; ^b angle φ between the main symmetry axis and a line from the central Au atom to a chlorine ligand (Fig. 4a); ^c for the coordination mode, see Fig. 4b; ^d distance between Cl and its closest Au neighbor; ^e distance to the second-nearest Au atom; for hollow coordination, there are two $\text{Au}^2\text{-Cl}$ bonds; ^f average Au–Au bond length; ^g binding energy per Cl atom; ^h vibrational frequencies ν of Au–Cl modes from a restricted normal mode analysis with a fixed Au_{55} core in S_6 symmetry; ⁱ total charge of the Cl_6 ligand shell from a Mulliken analysis.

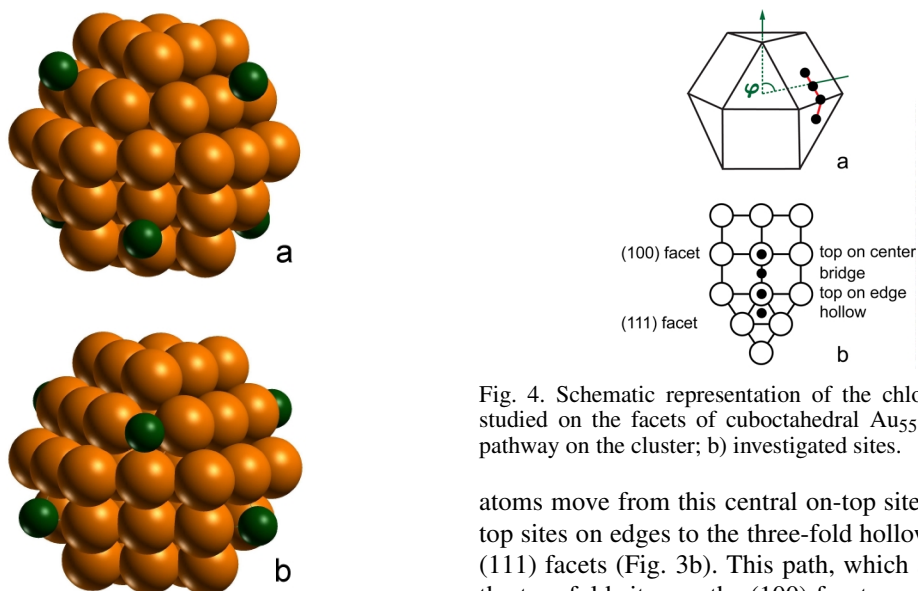


Fig. 3. Cluster $\text{Au}_{55}\text{Cl}_6$: a) Cl on top on (100) facets; b) Cl at bridge-hollow sites of (111) facets.

Chlorine coordination on Au_{55}

We examined chlorine coordination at cuboctahedral Au_{55} before addressing the full model cluster compound. EXAFS results for $\text{Au}_{55}[\text{P}(\text{C}_6\text{H}_5)_3]_{12}\text{Cl}_6$ served as reference: $\text{Au-Cl} = 250$ pm, Cl coordination number = 2.3 ± 1 [11]. Exploratory calculations on $\text{Au}_{55}\text{Cl}_6$ showed that Cl coordination on top of the central Au atoms of the (100) facets of cuboctahedral Au_{55} (Fig. 3a), as proposed for the compound $\text{Au}_{55}[\text{P}(\text{C}_6\text{H}_5)_3]_{12}\text{Cl}_6$ [9], is a local energy maximum with regard to lateral movement of the ligands. Therefore, we decided to scan the energy profile of $\text{Au}_{55}\text{Cl}_6$ in D_{3d} symmetry along a path (Fig. 4a) where the Cl

Fig. 4. Schematic representation of the chlorine positions studied on the facets of cuboctahedral Au_{55} . a) Sketch of pathway on the cluster; b) investigated sites.

atoms move from this central on-top sites *via* the on-top sites on edges to the three-fold hollow sites of the (111) facets (Fig. 3b). This path, which also includes the two-fold sites on the (100) facets, can be parameterized by the angle φ between the main C_3 axis and the line from the center of the cluster to one Cl ligand (Fig. 4a).

Nearest-neighbor distances $\text{Au}^1\text{-Cl}$ vary strongly with the coordination mode – from 231 pm for the strongest bound top sites at the edges between adjacent facets to 256 pm at hollow sites of the (111) facets (Table 3). The $\text{Au}^1\text{-Cl}$ distance increases by ~ 10 pm per coordinated Au atom. The average Au–Au distance increases concomitantly, but overall varies by only 3 pm. The distances $\text{Au}^2\text{-Cl}$ from the ligand to the second-nearest Au centers are also listed in Table 3 to demonstrate the symmetry of the two-fold sites on Au(100) facets and the three-fold sites on Au(111) facets. According to the calculated energies BE (Table 3), on-top adsorption complexes are the least stable ones along

the path scanned. Without crossing a barrier, a Cl ligand gains 42 kJ mol^{-1} on moving to a bridge position where it reaches the lowest point along the path explored, with $\text{BE} = 246 \text{ kJ mol}^{-1}$. Cl ligands on top of edge sites are only 6 kJ mol^{-1} more bound than at the central (100) top sites while ligation at the hollow position of the (111) facets is almost as stable as in a bridge complex, $\text{BE} = 234 \text{ kJ mol}^{-1}$ (Table 3).

To characterize approximately the local movements of the chlorine centers, we carried out a restricted normal mode analysis at the stationary points along the path just described (Fig. 4, Table 3), keeping the Au_{55} cluster core fixed. With symmetry constraints reduced to subgroup S_6 of D_{3d} , Cl vibrations in both directions parallel to the surface of the metal moiety are feasible, along the path and perpendicular to the mirror plane that contains the path. The frequency of the radial mode of a chlorine atom, perpendicular to that surface, varies notably with the site. As expected, higher values were determined at top coordinated sites ($308, 285 \text{ cm}^{-1}$), lower ones at the bridge (244 cm^{-1}) and the three-fold hollow site, (218 cm^{-1}). Top coordination at the center of the (100) facet yields two imaginary frequencies, hence is a local maximum with respect to lateral displacements. The two structures involving higher coordinated chlorine atoms (bridge, three-fold) are local minima of the potential energy surface. The top-coordinated site on the edge between the (100) and (111) facets is a saddle point of first order with the negative curvature directed along the edge. Thus, along the path depicted in Fig. 4a, one calculates a minimum for Cl at the top site of the edge. The latter finding may come as a surprise; it is associated with two changes of the electronic configuration on the way from the neighboring bridge site to the subsequent hollow site. The electron density withdrawn from the Au_{55} cluster by the chlorine ligand shell correlates inversely with the Au coordination of the ligation site: -1.5 e for top coordination, -0.9 e at the bridge, and -0.5 e at the hollow site.

These findings were checked by slab model calculations using a pseudopotential plane-wave based LDA supercell method on models of Cl adsorption at the ideal Au(100) and Au(111) surfaces. On Au(100), two-fold bridge sites were calculated as most stable; the binding energy was determined $\sim 48 \text{ kJ mol}^{-1}$ per adsorbate higher than for complexes with terminal chlorine coordination. The second most stable adsorption complex on Au(100) is at the three-fold hollow site; adsorbate binding is 7 kJ mol^{-1} less strong than at the

bridge site. The frequencies of the vibrational motion perpendicular to the surface compare within $\sim 5 \text{ cm}^{-1}$ with the corresponding results of the cluster models. The normal mode of Cl coordinated on top of Au(100), 281 cm^{-1} , is very similar to the corresponding cluster result. Essentially the same match holds for the frequency of the radial motion of Cl at the bridge site of Au(100), 239 cm^{-1} , and between the hollow site on the Au_{55} cluster and the hcp site of the Au(111) surface, 212 cm^{-1} . In summary, the calculated vibrational frequencies of Cl adsorption complexes on the cluster Au_{55} on the one hand and at the surfaces Au(100) and Au(111) on the other hand agree very well.

Finally, we mention clusters of size Au_{13} and Au_{39} where X-ray analysis revealed a terminal-like coordination of Cl ligands [66, 67]. However, these metal clusters do not exhibit surface facets, rather the Cl ligands are attached at corner and edge sites of a buckled surface. Hence the structures of these clusters are essentially different from that of Au_{55} .

Model cluster $\text{Au}_{55}(\text{PH}_3)_{12}\text{Cl}_6$

We studied the structure of the model cluster $\text{Au}_{55}(\text{PH}_3)_{12}\text{Cl}_6$ for selected Cl sites as the size of this problem did not allow an exhaustive search of all possible sites of chlorine at the cluster $\text{Au}_{55}(\text{PH}_3)_{12}$. In all structures studied (Fig. 2), the model phosphine ligands PH_3 were placed at corner atoms of Au_{55} and chlorine ligands were separated at least 320 pm from the closest hydrogen of the PH_3 groups. We used a model of D_{2d} symmetry to explore the structure originally proposed where the chlorine atoms were assigned to the centers of the (100) facets of Au_{55} (Fig. 2a) [9]. To model Cl at bridge sites on (100) facets or threefold-hollow sites on (111) facets (Fig. 2b), we used a cluster model of S_6 symmetry. This symmetry restriction allows one to study all arrangements of six symmetry equivalent chlorine centers. Yet, even this low symmetry is idealized because one can imagine chlorine atoms to assume in general locations independently of each other. We refrained from investigating four-fold sites on the (100) facets as they are expected to be affected rather strongly by steric hindrance from the triphenylphosphine ligands. For similar reasons, we also excluded top sites on edges.

For all models rather similar binding energies per Cl ligand have been calculated, ranging from 226 kJ mol^{-1} for top coordination to 251 kJ mol^{-1} for hollow coordination on a cluster model with S_6

Table 4. Calculated properties of various isomers of the model cluster Au₅₅(PH₃)₁₂Cl₆. For comparison corresponding results are shown for the clusters Au₅₅ and Au₅₅(PH₃)₁₂.

Symmetry Cl coordination	Au ₅₅	Au ₅₅ (PH ₃) ₁₂	Au ₅₅ (PH ₃) ₁₂ Cl ₆					exp.
	S ₆	D _{2d}	D _{2d} α ^a	D _{2d} β ^a	S ₆ ^a	S ₆ α ^a	S ₆ β ^b	
(Au–Au) ^c , pm	280.3	277.9	278.2	278.3	279.9	282.8	280.1	275–280 ^d
Au–P, pm		230.9	230.1	230.0	231.7	230.4	231.5	230
Au ¹ –Cl ^e , pm			238.1	237.9	249.1	258.2	251.2	250
Au ² –Cl ^e , pm			240.0	238.8	251.0	260.3	263.6	
Au ³ –Cl ^e , pm			–	–	–	262.2	268.0	
E _{rel} ^f , kJ mol ^{−1}			153	151	100	79	0	
BE ^g , kJ mol ^{−1}			226	226	234	238	251	
Δε ^h , eV	0.14	0.06	0.37	0.02	0.12	0.25	0.17	
IP ^j , eV	6.18	4.46	4.83	4.86	4.69	4.74	4.60	
EA ^k , eV	3.93	2.44	2.91	2.87	2.75	2.79	2.60	
M ^l	2	2	2	4	2	2	2	
q[Au ₅₅] ^m , e		−0.3	1.5	1.4	1.3	0.5	0.7	
q[(PH ₃) ₁₂] ^m , e		0.3	0.8	0.8	0.5	0.7	0.5	
q[Cl ₆] ^m , e			−2.3	−2.3	−1.7	−1.3	−1.2	

^a Cuboctahedral; ^b icosahedral; ^c average Au–Au bond length; ^d refs. [11–13]; ^e distance between Cl and different Au atoms nearby; ^f energy difference to the most stable model cluster; ^g binding energies per chlorine atom; ^h HOMO-LUMO gap; ^j ionization potential; ^k electron affinity; ^l multiplicity; ^m Mulliken charges.

symmetry (Table 4). With one exception, all models of Au₅₅(PH₃)₁₂Cl₆ essentially preserve the octahedral shape of the Au₅₅ metal core. However, the most stable structure S₆β with Cl at threefold hollow positions adopts a quasi-icosahedral structure where the (100) facets are bent along their diagonal by 40° (Fig. 2c). In an ideal icosahedron this angle between adjacent surface triangles is 45°. Isomer S₆α with the same Cl coordination, but octahedral symmetry of the Au₅₅ metal core, yields a lower ligand binding energy, 238 kJ mol^{−1}, which corresponds to a total energy difference of 79 kJ mol^{−1} with respect to model S₆β (Table 4). Bridge coordination of Cl leads to a similar ligand binding energy, 234 kJ mol^{−1}. With a total energy difference of only 2 kJ mol^{−1}, the two isomers with Cl in top coordination (D_{2d} symmetry) are degenerate, despite of different spin states (doublet and quartet, Table 4); they feature the lowest binding energy, 226 kJ mol^{−1}.

As for Au₅₅Cl₆, in the fully ligated models the Au–Cl bond lengths of the octahedral species increase with the coordination number, from 238 pm for top coordination to 250 pm at the bridge position to ~260 pm for the threefold-hollow position (Table 4). In contrast, at the threefold hollow positions of the quasi-icosahedral species S₆β, one Au–Cl bond is notably shorter, 251 pm, than the other two contacts, 264 pm and 268 pm. On the cluster compound S₆α Cl occupies the hollow site in a rather symmetric way, 258–262 pm. In the presence of the phosphine ligands,

the Cl bond lengths are 4–5 pm longer than in Au₅₅Cl₆ (Tables 3, 4). Au–P bonds are remarkably stable with respect to different positions of the Cl ligands. They vary between 230 and 232 pm, in perfect agreement with the experimental value, 230 pm [11]. Also average Au–Au distances increase only slightly due to Cl coordination, from 278 pm for on-top Cl deposition to 280–282 pm for the higher coordinated sites (Table 4). These values are at most 1 pm larger than for the model Au₅₅Cl₆ (Table 3), despite the relatively strong distortions of the metal cluster core in the most stable species S₆β (Fig. 2c).

Comparison of the calculated structures with experiment is quite limited. Only the Au–Cl bonds of Au₅₅(PH₃)₁₂(μ₂-Cl)₆ S₆ compare well with the experimental result, 250 pm [11]. For cluster models with Cl at μ₃ (hollow) sites, the short Au–Cl distance, 251 pm, also matches the experimental value. However, EXAFS experiments should be able to detect also the other Au–Cl distances, up to ~268 pm, if that structure were present. Top coordination of Cl, with computed Au–Cl bonds of ~238 pm, is at variance with EXAFS results [11]. The experimental value of Au–P, 230 ± 2 pm, is well reproduced by all cluster models studied; the corresponding computational results, ranging from 230 pm to 232 pm, fall within the error margin of the experiment. The computed average Au–Au distances, 278–283 pm (Table 4), are compatible with the larger values determined experimentally, 280 [12], 278.5 [13], and 275 pm [11].

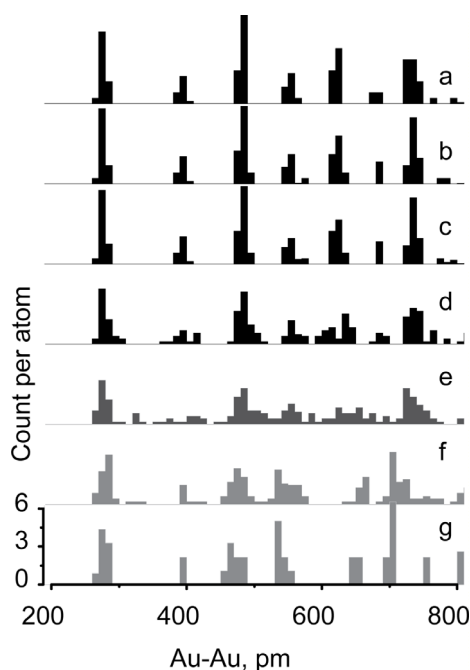


Fig. 5. Radial distribution functions of Au atoms as histograms (bin width 10 pm) of various $\text{Au}_{55}(\text{PH}_3)_{12}\text{Cl}_6$ cluster models compared to bare Au_{55} clusters in O_h and I_h symmetry. a) $\text{Au}_{55} O_h$; b) $\text{Au}_{55}(\text{PH}_3)_{12}(\mu_1\text{-Cl})_6 D_{2d}\alpha$; c) $\text{Au}_{55}(\text{PH}_3)_{12}(\mu_1\text{-Cl})_6 D_{2d}\beta$; d) $\text{Au}_{55}(\text{PH}_3)_{12}(\mu_2\text{-Cl})_6 S_6$; e) $\text{Au}_{55}(\text{PH}_3)_{12}(\mu_3\text{-Cl})_6 S_6\alpha$; f) $\text{Au}_{55}(\text{PH}_3)_{12}(\mu_3\text{-Cl})_6 S_6\beta$; g) $\text{Au}_{55} I_h$. For details on counting the Au–Au contacts, see text.

The second and third shells of Au–Au distances have been also reported from experiment [11]; therefore, we analyzed the distributions of nearest-neighbor Au–Au distances of all Au centers in the model clusters studied. Fig. 5 displays the histograms (bin width 10 pm) that result from counting the number of Au–Au distances per Au atom. Multiplication by the factor $2/55$ yields the values displayed which are normalized to a single Au atom as reference.

The histograms of the cluster models with cuboctahedral cluster core, Au_{55} , $\text{Au}_{55}(\text{PH}_3)_{12}(\mu_1\text{-Cl})_6\alpha$, and $\text{Au}_{55}(\text{PH}_3)_{12}(\mu_1\text{-Cl})_6\beta$, apparently are very similar (Figs. 5a, b, c). Thus metal cores of the two D_{2d} structures of $\text{Au}_{55}(\text{PH}_3)_{12}\text{Cl}_6$ remain close to the shape of an ideal cuboctahedron. This result also illustrates the overall structural similarity of the two spin states of D_{2d} symmetry. The model $\text{Au}_{55}(\text{PH}_3)_{12}(\mu_2\text{-Cl})_6 S_6$, with Cl ligands at bridge sites, generates a pattern similar to those of the cuboctahedral models, but the peaks are slightly broadened (Fig. 5d). In contrast, the main features of the radial distribution function

of $\text{Au}_{55}(\text{PH}_3)_{12}(\mu_3\text{-Cl})_6 S_6\alpha$, the quasi-cuboctahedral cluster model with S_6 symmetry, are distinctly broadened (Fig. 5e), reflecting the distortion of the cluster structure. The quasi-icosahedral isomer of S_6 symmetry, $\text{Au}_{55}(\text{PH}_3)_{12}(\mu_3\text{-Cl})_6 S_6\beta$, exhibits a radial distribution function with peaks that are clearly shifted with respect to the distributions of the cuboctahedral clusters (Fig. 5f). Nevertheless, all structures reproduce reasonably well the experimentally found first shell, with values between 270 and 280 pm. At the resolution of the histogram, inter- and intra-shell distances of the quasi-icosahedral structures do not differ in a significant way.

The radial distribution functions of all structures, except $\text{Au}_{55}(\text{PH}_3)_{12}(\mu_3\text{-Cl})_6 S_6\alpha$ (Fig. 5e), feature a second pronounced shell at 390 pm, in excellent agreement with experiment, 393 pm [11]. In all structures one notes a third peak near 470–480 pm, which also matches experiment, 488 pm [11]. Leaving aside the structure of the quasi-cuboctahedral cluster $\text{Au}_{55}(\text{PH}_3)_{12}(\mu_3\text{-Cl})_6 S_6\alpha$, one notes an overall very good agreement for the Au–Au distances. The deviations of 5% between inter- and intra-shell distances of an ideal icosahedron are reflected only in some broadening of the peaks, but not as distinctive patterns in the calculated distribution functions. Hence, detection of inter- and intra-shell distances by EXAFS seems quite unlikely. A clear distinction of these Au–Au distances can only be expected if the metal centers are distributed uniformly. This is the case for small clusters with an icosahedral structural motif, *e.g.* with 13 or less metal centers (see Introduction). However, in view of the perturbation by the ligands one should not expect the metal core of a large ligated cluster like $\text{Au}_{55}[\text{P}(\text{C}_6\text{H}_5)_3]_{12}\text{Cl}_6$ to feature such an ideal shape.

Finally, note that the radial distribution functions of the quasi-cuboctahedral and quasi-icosahedral clusters essentially agree for the first three shells (Figs. 5a, g). The various distributions differ notably in the position of the fifth shell which peaks near 620 pm for all cuboctahedral structures, but at ~ 650 pm for icosahedral clusters. However, with EXAFS interatomic distances of 600 pm or beyond are not easily measured in an accurate way [11, 13, 86, 69].

After analyzing the structures and the stability of the various cluster models, we now discuss some calculated electronic properties (Table 4). The HOMO-LUMO gap varies only slightly among the cluster models studied. The largest gap, 0.37 eV, is calculated for the doublet state with top coordinated Cl ligands, while

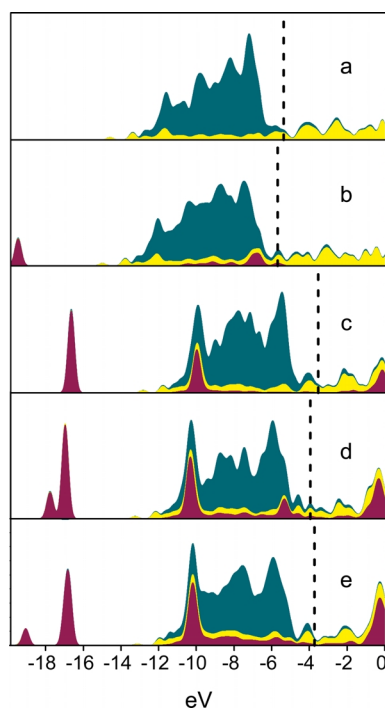


Fig. 6. Density of states (in arbitrary units) of various cluster models: a) $\text{Au}_{55} O_h$; b) $\text{Au}_{55}(\mu_1\text{-Cl})_6 O_h$; c) $\text{Au}_{55}(\text{PH}_3)_{12} D_{2d}$; d) $\text{Au}_{55}(\text{PH}_3)_{12}(\mu_1\text{-Cl})_6 D_{2d}\alpha$; e) $\text{Au}_{55}(\text{PH}_3)_{12}(\mu_3\text{-Cl})_6 S_6\beta$. The dashed lines indicate the Fermi level of each system. Contributions of the ligands – purple, Au *sp* – yellow, Au *d* – green (color online).

the corresponding quartet state results in the smallest gap, 0.02 eV. Cl ligands at higher coordinated sites lead to gaps of 0.1–0.2 eV. The ionization potential and the electron affinity of clusters with top Cl ligands are ~ 0.1 eV larger than for models with Cl ligands at higher coordinated sites. As already noted for the model $\text{Au}_{55}(\text{PH}_3)_{12}$, phosphine ligands in general strongly reduce the IP and the EA of $\text{Au}_{55}(\text{PH}_3)_{12}\text{Cl}_6$, at least by 1.3 and 1.0 eV, respectively, compared to bare Au_{55} . Both, IP and EA show weak trends to lower values with increasing stability of the cluster compound; these variations unfortunately are too small to assist in discriminating structures experimentally. The Mulliken charges are as expected from coordination chemistry. The Cl ligands withdraw electron density from the metal particle, while PH_3 ligands donate density. Compared to $\text{Au}_{55}\text{Cl}_6$ (Table 3), the charge on the metal moiety of $\text{Au}_{55}(\text{PH}_3)_{12}\text{Cl}_6$ does not change when phosphines are attached. The electron density donated to the cluster by the PH_3 ligands overall is transferred to the Cl ligand shell (Table 4).

Density of states (DOS) plots (Fig. 6) provide an overview of the valence electronic structure. Recall that the Kohn-Sham energies from approximate exchange-correlation potentials in general differ from ionization energies [51]. The *d*-manifold of the Au moiety dominates the region between -7 eV and -12 eV, whereas the DOS at the Fermi edge consists of *s*-type levels. As the calculations did not account for the spin-orbit interaction, comparison of the Au *5d* manifold with experiment should be done with due caution. The effect of terminally coordinated Cl ligands on the DOS is small. Only the Fermi energy is slightly shifted to a lower value (in absolute terms); also, at about -7 eV, the Cl *3p* levels appear as a shoulder on the Au *5d* manifold. The Cl *3s* levels form a small peak near -20 eV. In agreement with the effect on the ionization potential (Table 4), phosphine ligands induce a strong upward shift, by ~ 2 eV, of the DOS and the Fermi energy. One notices two peaks, at about -17 eV and -10 eV, that are related to the PH_3 ligands. The phosphine induced shifts of the Au *5d* manifold and the Fermi energy of Au_{55} are also observed for the fully ligated species $\text{Au}_{55}(\text{PH}_3)_{12}(\mu_1\text{-Cl})_6 D_{2d}\alpha$ (Fig. 6d); the other spin isomer, $\text{Au}_{55}(\text{PH}_3)_{12}(\mu_1\text{-Cl})_6 D_{2d}\beta$, exhibits essentially the same DOS. Phosphine coordination also uniformly shifts all Cl-related features of the DOS to lower energies, by ~ 2 eV. The DOS of $\text{Au}_{55}(\text{PH}_3)_{12}(\mu_2\text{-Cl})_6 S_6$ is very similar to the DOS of the models $\text{Au}_{55}(\text{PH}_3)_{12}\text{Cl}_6$ with D_{2d} symmetry (Fig. 6d) except for the Cl contributions. The DOS of the two S_6 isomers with Cl ligands at hollow positions are rather similar (Fig. 6e depicts $\text{Au}_{55}(\text{PH}_3)_{12}(\mu_3\text{-Cl})_6 S_6\beta$), despite the different geometry of the metal core (see above).

The energy of the Fermi level correlates with the ionization potential as is to be expected [51] if self-interaction artifacts due to the approximate exchange-correlation potential are comparable for the systems inspected. The HOMO of the cluster compound is destabilized when phosphine ligands are coordinated, while chlorine coordination has a small effect in the opposite direction. In experiment, the ultraviolet photoelectron spectrum was observed to change at the Fermi level upon removal of chlorine ligands [23]. The calculated DOS of the model $\text{Au}_{55}(\text{PH}_3)_{12}$ (Fig. 6c) is lower at the Fermi level, and all fully coordinated species show a similar DOS. An insulator-to-metal transition had been associated with changes of the experimental DOS upon removal of Cl ligands [23], but we were unable to identify similar changes in the calculated DOS upon go-

ing from $\text{Au}_{55}(\text{PH}_3)_{12}\text{Cl}_6$ to $\text{Au}_{55}(\text{PH}_3)_{12}$. Indeed, removal of Cl ligands may cause unidentified changes in the structure of the sample and hence in the interaction between neighboring cluster compounds. However, from the present results, we are unable to identify signatures of a metal-to-insulator transition.

Summary

Using relativistic density functional calculations on model clusters $\text{Au}_{55}(\text{PH}_3)_{12}\text{Cl}_6$, we explored geometric and electronic properties of various structures of the proposed cluster compound $\text{Au}_{55}[\text{P}(\text{C}_6\text{H}_5)_3]_{12}\text{Cl}_6$. The shape of the metal moiety and the coordination of the Cl ligands were varied whereas the phosphine ligands in all models were assumed to be coordinated on top of Au corner atoms. The originally suggested structure [9] with terminal Cl coordination on top of Au centers of (100) facets was calculated to be a local energy maximum for lateral movement and energetically unfavorable, with an Au–Cl binding energy of 226 kJ mol^{-1} . The binding energy of bridge-coordinated Cl ligands at (100) facets was calculated higher, at 234 kJ mol^{-1} . Even larger Au–Cl binding energies resulted for Cl ligands at three-fold sites, 238 kJ mol^{-1} on a cuboctahedral and 251 kJ mol^{-1} on a quasi-icosahedral cluster core. Au–Cl bond lengths were calculated to increase by $\sim 10 \text{ pm}$ per neighboring Au center: from $\sim 240 \text{ pm}$ for terminal, to $\sim 250 \text{ pm}$ for two-fold, and $\sim 260 \text{ pm}$ for three-fold coordinated Cl ligands. EXAFS data agree favorably with the two latter values for higher coordinated sites. When Cl ligands are attached at three-fold sites of an octahedral Au_{55} structure, the metal moiety relaxes notably to form a quasi-icosahedral cluster; the concomitant energy gain is 79 kJ mol^{-1} . For all species studied, the model phosphine ligands PH_3 are attached *via* Au–P bonds of 230 pm , in good agreement with EXAFS data. These phosphine ligands donate electron density to the cluster, shifting the DOS (including the HOMO) to lower binding energies. In consequence, ionization potential and electron affinity are calculated to be reduced by $\sim 1 \text{ eV}$.

Comparison to EXAFS results shows that the calculated shells of Au–Au distances fit equally well both cuboctahedral and icosahedral cluster models. For all structures studied, calculations reproduce the first three shells within 10 pm of the experimental values, 275 pm , 393 pm , and 488 pm . The only exception is the structure of the distorted cuboctahedral cluster $\text{Au}_{55}(\text{PH}_3)_{12}(\mu_3\text{-Cl})_6 S_6\alpha$.

In summary, from this computational study one concludes that Cl ligands of the cluster compound $\text{Au}_{55}[\text{P}(\text{C}_6\text{H}_5)_3]_{12}\text{Cl}_6$ are higher coordinated, at variance with the earlier suggestion of terminal coordination [9]. Structural and energetic aspects of the present calculations favor a (quasi-) icosahedral shape of the Au_{55} cluster core over a distorted cuboctahedral structure. Thus, the calculated results corroborate the hypothesis [21, 22] that the cluster compound $\text{Au}_{55}[\text{P}(\text{C}_6\text{H}_5)_3]_{12}\text{Cl}_6$ features a distorted metal moiety of quasi-icosahedral shape. One should keep in mind that Cl ligands at hollow sites may not follow a high-symmetry pattern, as assumed in the present models. Rather, in the samples studied experimentally, the six Cl ligands may to some extent be randomly distributed on the hollow sites of 20 suitable triangular facets of a quasi-icosahedral metal moiety. An ensemble of isomers results, but the clusters of a given sample may not even be stoichiometrically identical.

$\text{Au}_{55}[\text{P}(\text{C}_6\text{H}_5)_3]_{12}\text{Cl}_6$ is one of the few better characterized large cluster compounds. Ever since its first synthesis [9], this compound stimulated many studies to uncover its structure and other properties [10–13, 17, 18, 20–22, 28–31, 34]. The present computational results indicate that further experimental work, especially regarding the shape, and the ligand coordination of the metal core, is required to achieve a full characterization of this cluster compound. Finally, we hope that the results obtained for the model cluster $\text{Au}_{55}(\text{PH}_3)_{12}\text{Cl}_6$ may also serve as useful reference when studying similar cluster compounds.

Acknowledgements

Over the years, N. R. and S. K. enjoyed numerous stimulating discussions with Prof. Hubert Schmidbaur, in particular on gold cluster compounds. The dedication of this paper to Prof. Schmidbaur on the occasion of his 75th birthday is but a modest sign of gratitude for these fruitful interactions. In fact, the desire to calculate the electronic structure of a carbon-centered hexa-gold cluster compound, synthesized by Prof. Schmidbaur and his co-workers, ultimately lead N. R. and his group to develop a very efficient procedure for solving the relativistic Kohn-Sham equation of density functional theory. The present work also employed that approach, based on the Douglas-Kroll-Hess method. We also would like to thank Alena Kremleva for carrying out the slab-model calculations on the adsorption of chlorine atoms at gold surfaces. Computer time provided by the Leibniz Rechenzentrum München is gratefully acknowledged. This work was supported by the Fonds der Chemischen Industrie.

- [1] P. Braunstein, L. A. Oro, P. R. Raithby (Eds.), *Metal Clusters in Chemistry*, Wiley-VCH, Weinheim, **1999**.
- [2] M.-C. Daniel, D. Astruc, *Chem. Rev.* **2004**, *104*, 293.
- [3] G. Schmid (Ed.), *Clusters and Colloids. From Theory to Applications*, VCH Verlagsgesellschaft mbH, Weinheim, **1994**.
- [4] A. C. Templeton, W. P. Wuefeling, R. W. Murray, *Acc. Chem. Res.* **2000**, *33*, 27.
- [5] M. Haruta, *Nature* **2005**, *437*, 1098.
- [6] M. D. Hughes, Y.-J. Xu, P. Jenkins, P. McMorn, P. Landon, D. I. Enache, A. F. Carley, G. A. Attard, G. J. Hutchings, F. King, E. H. Stitt, P. Johnston, K. Griffin, C. J. Kiely, *Nature* **2005**, *437*, 1132.
- [7] D. W. Goodman, *Nature* **2008**, *454*, 948.
- [8] M. Turner, V. B. Golovko, O. P. H. Vaughan, P. Abdulkhin, A. Berenguer-Murcia, M. S. Tikhov, B. F. G. Johnson, R. M. Lambert, *Nature* **2008**, *454*, 981.
- [9] G. Schmid, R. Pfeil, R. Boese, F. Bandermann, S. Meyer, G. H. M. Calis, J. W. A. van der Velden, *Chem. Ber.* **1981**, *114*, 3634.
- [10] R. C. Thiel, R. E. Benfield, R. Zanoni, H. H. A. Smit, M. W. Dirken, *Structure and Bonding* **1993**, *81*, 1.
- [11] P. D. Cluskey, R. J. Newport, R. E. Benfield, S. J. Gorman, G. Schmid, *Supplement to Z. Phys. D* **1993**, *26*, S 8.
- [12] M. A. Marcus, M. P. Andrews, J. Zegenhagen, A. S. Bommanavar, P. Montano, *Phys. Rev. B* **1990**, *42*, 3312.
- [13] R. E. Benfield, D. Grandjean, M. Kröll, R. Pugin, T. Sawitowski, G. Schmid, *J. Phys. Chem. B* **2001**, *105*, 1961.
- [14] O. D. Häberlen, S.-C. Chung, M. Stener, N. Rösch, *J. Chem. Phys.* **1997**, *106*, 5189.
- [15] R. C. Weast (Ed.), *CRC Handbook of Chemistry and Physics*, 64 ed. CRC Press, Boca Raton; FL, **1983**.
- [16] A. S. Barnard, L. A. Curtiss, *Chem. Phys. Chem.* **2006**, *7*, 1544.
- [17] J. P. Fackler, Jr., C. J. McNeal, R. E. P. Winpenny, L. H. Pignolet, *J. Am. Chem. Soc.* **1989**, *111*, 6434.
- [18] C. J. McNeal, R. E. P. Winpenny, J. M. Hughes, R. D. Macfarlane, L. H. Pignolet, L. T. J. Nelson, T. G. Gardner, L. H. Irgens, G. Vigh, J. P. Fackler, Jr., *Inorg. Chem.* **1993**, *32*, 5582.
- [19] R. Balasubramanian, R. Guo, A. J. Mills, R. W. Murray, *J. Am. Chem. Soc.* **2005**, *127*, 8126.
- [20] G. Schmid, *Chem. Rev.* **1992**, *92*, 1709.
- [21] W. Vogel, B. Rosner, B. Tesche, *J. Phys. Chem.* **1993**, *97*, 11611.
- [22] D. H. Rapoport, W. Vogel, H. Cölfen, R. Schlögl, *J. Phys. Chem. B* **1997**, *101*, 4175.
- [23] H.-G. Boyen, G. Kästle, F. Weigl, P. Ziemann, G. Schmid, M. G. Garnier, P. Oelhafen, *Phys. Rev. Lett.* **2001**, *87*, 276401.
- [24] G. Schmid, L. F. Chi, *Adv. Mater.* **1998**, *10*, 515.
- [25] H. Feld, A. Leute, D. Rading, A. Benninghoven, *J. Am. Chem. Soc.* **1990**, *112*, 8166.
- [26] H. Feld, A. Leute, D. Rading, A. Benninghoven, *Z. Phys. D* **1990**, *17*, 73.
- [27] G. Schmid, *Chem. Soc. Rev.* **2008**, *37*, 1909.
- [28] R. E. Benfield, J. A. Creighton, D. G. Eadon, G. Schmid, *Z. Phys. D* **1989**, *12*, 533.
- [29] R. C. Thiel, R. E. Benfield, R. Zanoni, H. H. A. Smit, M. W. Dirken, *Z. Phys. D* **1993**, *26*, 162.
- [30] K. Fauth, U. Kreibitz, G. Schmid, *Z. Phys. D* **1989**, *12*, 515.
- [31] H. B. Brom, M. P. J. Van Staveren, L. J. De Jongh, *Z. Phys. D* **1991**, *20*, 281.
- [32] P. Joyes, *Z. Phys. D* **1995**, *32*, 337.
- [33] H. B. Brom, J. Baak, L. J. De Jongh, F. M. Mulder, R. C. Thiel, G. Schmid, *Supplement to Z. Phys. D* **1993**, *26*, S. 27.
- [34] H. Zhang, U. Hartmann, G. Schmid, *Appl. Phys. Lett.* **2004**, *84*, 1543.
- [35] H. Zhang, D. Mautes, U. Hartmann, *New J. Phys.* **2003**, *5*, 30.
- [36] G. Schmid, B. Corain, *Eur. J. Inorg. Chem.* **2003**, *17*, 3081.
- [37] G. Schmid, *Adv. Eng. Mater.* **2001**, *3*, 737.
- [38] H. Zhang, G. Schmid, U. Hartmann, *Nano Lett.* **2003**, *3*, 305.
- [39] B. I. Dunlap, N. Rösch, *Adv. Quantum Chem.* **1990**, *21*, 317.
- [40] Th. Belling, T. Grauschopf, S. Krüger, M. Mayer, F. Nörtemann, M. Staufer, C. Zenger, N. Rösch in *High Performance Scientific and Engineering Computing, Proceedings of the First International FORTWIHR Conference 1998, Lecture Notes in Computational Science and Engineering*, Vol. 8 (Eds.: H.-J. Bungartz, F. Durst, C. Zenger), Springer, Heidelberg **1999**, p. 439.
- [41] Th. Belling, T. Grauschopf, S. Krüger, F. Nörtemann, M. Staufer, M. Mayer, V. A. Nasluzov, U. Birkenheuer, A. Shor, A. Matveev, A. Hu, M. S. K. Fuchs-Rohr, K. M. Neyman, D. I. Ganyushin, T. Kerdcharoen, A. Woiterski, N. Rösch, PARAGAUSS (version 2.2), Technische Universität München, München (Germany) **2001**.
- [42] O. D. Häberlen, N. Rösch, *Chem. Phys. Lett.* **1992**, *199*, 491.
- [43] N. Rösch, S. Krüger, M. Mayer, V. A. Nasluzov in *Theoretical and Computational Chemistry, Recent Developments and Applications of Modern Density Functional Theory*; (Ed.: J. Seminario), Elsevier, Amsterdam, **1996**, p. 497.
- [44] N. Rösch, A. V. Matveev, V. A. Nasluzov, K. M. Neyman, L. Moskaleva, S. Krüger, in *Relativistic Electronic Structure Theory – Applications*,

- Theoretical and Computational Chemistry Series* (Ed.: P. Schwerdtfeger), Elsevier, Amsterdam, **2004**, p. 656.
- [45] S. Vosko, L. Wilk, M. Nusair, *Can. J. Phys.* **1980**, *58*, 1200.
- [46] A. D. Becke, *Phys. Rev. A* **1988**, *38*, 3098.
- [47] J. P. Perdew, *Phys. Rev. B* **1986**, *33*, 8822; J. P. Perdew, *Phys. Rev. B* **1986**, *34*, 7406.
- [48] S. Krüger, M. Stener, N. Rösch, *J. Chem. Phys.* **2001**, *114*, 5207.
- [49] V. A. Nasluzov, N. Rösch, *Chem. Phys.* **1996**, *210*, 413.
- [50] O. D. Häberlen, S.-C. Chung, N. Rösch, *Int. J. Quantum Chem.* **1997**, *106*, 5189.
- [51] A. Görling, S. B. Trickey, P. Gisdakis, N. Rösch in *Topics in Organometallic Chemistry*, Vol. 4 (Eds.: J. Brown, P. Hofmann), Springer, Heidelberg, **1999**, p. 109.
- [52] A. D. Becke, *J. Chem. Phys.* **1988**, *88*, 2547.
- [53] V. I. Lebedev, *Zh. Vychisl. Mat. Mat. Fiz.* **1976**, *16*, 293.
- [54] Au: O. D. Häberlen, S.-C. Chung, N. Rösch, *Int. J. Quantum Chem., Quantum Chem. Symp.* **1994**, *28*, 595; Cl: Y. Sakai, H. Tatewaki, S. Huzinaga, *J. Comput. Chem.* **1981**, *2*, 108 [Cl: d exponent 0.56]; P: A. Veillard, *Theor. Chim. Acta* **1968**, *12*, 405; S. Huzinaga, J. Andzelm, M. Klobukowski, E. Radzio-Andzelm, Y. Sakai, H. Tatewaki, *Gaussian Basis Sets for Molecular Calculations*; Elsevier, Amsterdam, **1984**; H: s-exponents from F. B. Van Duijneveldt, *IBM Res. Rep. RJ 945* **1971**; p-exponent (1.0) from M. J. Frisch, J. A. Pople, J. S. Binkley, *J. Chem. Phys.* **1984**, *80*, 3265.
- [55] S. F. Boys, F. Bernardi, *Mol. Phys.* **1970**, *19*, 553.
- [56] S. M. Bishop, *Group Theory and Chemistry*, New York, Dover Publications, **1973**.
- [57] G. D'Agostino, A. Pinto, S. Mobilio, *Phys. Rev. B* **1993**, *48*, 14447.
- [58] I. Garzon, A. Posada-Amarillas, *Phys. Rev. B* **1996**, *54*, 11796.
- [59] J. M. Soler, M. R. Beltran, K. Michaelian, I. L. Garzon, P. Ordejon, D. Sanchez-Portal, E. Artacho, *Phys. Rev. B* **2000**, *61*, 5771.
- [60] D. Alamanova, V. G. Grigoryan, M. Springborg, *Z. Phys. Chem.* **2006**, *220*, 811.
- [61] O. D. Häberlen, N. Rösch, *J. Phys. Chem.* **1993**, *97*, 4970.
- [62] R. E. Benfield, A. Filipponi, D. T. Bowron, R. J. Newport, S. J. Gurman, *J. Phys: Condens. Matter* **1994**, *6*, 8429.
- [63] N. C. Baenziger, W. E. Bennett, D. M. Soborofe, *Acta Crystallogr. B* **1976**, *32*, 962.
- [64] K. Angermaier, E. Zeller, H. Schmidbaur, *J. Organomet. Chem.* **1994**, *472*, 371.
- [65] K. Angermaier, G. A. Bowmaker, E. N. de Silva, P. C. Healy, B. E. Jones, H. Schmidbaur, *J. Chem. Soc., Dalton Trans.* **1996**, *19*, 3121.
- [66] C. E. Briant, B. R. C. Theobald, J. W. White, L. K. Bell, D. M. P. Mingos, A. J. Welch, *J. Chem. Soc., Chem. Commun.* **1981**, 201.
- [67] B. K. Teo, X. Shi, H. Zhang, *J. Am. Chem. Soc.* **1992**, *114*, 2743.
- [68] C. Hennig, T. Reich, W. Kraus, G. Reck, F. Prokert, N. Schell, *Phys. Scr.* **2005**, *T115*, 352.
- [69] M. A. Denecke, *Coord. Chem. Rev.* **2006**, *250*, 730.